ARTICLES

Ultrasonication-Induced Formation of Silver Nanofibers in Reverse Micelles and Small-Angle X-ray Scattering Studies

Jianling Zhang, Buxing Han,* Minghua Liu, Dongxia Liu, Zexuan Dong, Jun Liu, and Dan Li

Center for Molecular Sciences, Institute of Chemistry, Chinese Academy of Sciences, Beijing 100080, P.R. China

Jun Wang, Baozhong Dong, Hui Zhao, and Lixia Rong

Institute of High Energy Physics, Chinese Academy of Sciences, Beijing 100039, P.R. China

Received: August 11, 2002; In Final Form: November 19, 2002

The Ag nanorods and nanofibers have been synthesized in sodium bis(2-ethylhexyl) sulfosuccinate (AOT)/isooctane reverse micelles with the aid of low-intensity ultrasonication. The TEM results show that only spherical silver nanoparticles can be obtained from the reverse micelles in the absence of ultrasonication whereas needle-shaped and wire-shaped silver particles are obtained as ultrasonication is applied. The possibility of ultrasonication to induce the aggregation of nanoparticles dispersed in reverse micelles is also confirmed by UV spectra. Small-angle X-ray scattering (SAXS) is used to obtain information on the microstructure change of the reverse micelles by ultrasonication. It is revealed that by ultrasonication the micelles change from a spherical to an ellipsoidal structure, of which the size can be tuned by the ultrasonication time.

1. Introduction

The synthesis of nanosized materials of a specific size and morphology is a key aspect in fields as diverse as modern materials,[1−4] catalysis,[5−7] electronics,[8−10] biotechnology,[11−13] and so forth. In particular, nanoparticles with high-order structures such as nanowires, nanofibers, and nanorods have attracted much attention because of their importance in both fundamental and potential applications in nanodevices.[14−16] For the fabrication of nanostructures of desired materials, the template method has been demonstrated to be very effective. Carbon nanotubes,[17−20] porous alumina,[21−23] and nanochannel glass[24,25] as hard templates have been widely used to control the size, the shape, and the alignment of nanoparticles.

Ultrasound has become an important tool in chemistry in recent years. It is well known that ultrasonic radiation in liquids has a variety of physical and chemical effects that are derived from acoustic cavitation, which can provide a unique method for driving chemical reactions under extreme conditions.[26] Diverse and promising applications of ultrasound such as the synthesis of nanostructured materials in various forms,[27−29] the preparation of biomaterials,[30,31] and modifications to polymers and polymer surfaces[32−3] have been exploited in materials chemistry.[4] Recently, many groups have reported the synthesis of nanorods or nanowires of inorganic materials using sonochemical methods.[35−38] For example, Nikitenko et al.[37−38] have successfully synthesized tungsten sulfide and tungsten oxide nanorods via ultrasonic irradiation of a solution of tungsten hexacarbonyl $W(CO)_6$ in diphenylmethane (DPhM) at 90 °C followed by heating and annealing processes at temperatures higher than 800 °C. In these methods, high-intensity ultrasonication (20 kHz) is needed to drive the chemical reaction that occurs under special conditions.

As organized media, the use of reverse micelles for nanoparticle synthesis has attracted much interest because of its potential advantages.[39−41] Because the reaction is restricted in the water core, the growth of the obtained product particles can be controlled by the size of the polar core, and the solid nanoparticles can be stabilized. In most cases, spherical nanoparticles are formed within the polar cores of reverse micelles. However, under certain conditions, further growth and aggregation of the initially formed nanoparticles result in the formation of higher-order structures such as needles,[42] fibers,[43] and wires.[44−46] This principle has been exemplified through a number of studies involving inorganic precipitation in bicontinuous microemulsions,[47−49] block copolymer micelles,[50−53] and other methods,[54,55] which are usually referred to as "soft template" methods for the synthesis of nanoparticles with high-order structures.

It is interesting and desirable to synthesize various nanostructures directly from the reverse micelles by a simple method. In this work, we propose a simple method to synthesize nanorods and nanofibers from sodium bis(2-ethylhexyl) sulfosuccinate (AOT)/isooctane reverse micelles with the aid of low-intensity ultrasonication. The effect of the ultrasonication on the microstructure of the reverse micelles is investigated by SAXS, which is a powerful technique that is used to study the properties of micellar solutions.[56−61] The results show that the micellar shape is transformed from a sphere to an ellipsoid by ultrasonication. We believe that study of the effect of ultrasonication on the

* To whom correspondence should be addressed. E-mail: Hanbx@infoc3.icas.ac.cn. Tel: 86-10-62562821. Fax: 86-10-62559373.

10.1021/jp026738f CCC: $25.00
Published on Web 03/22/2003

properties of the reverse micelles and the related applications are new and interesting topics.

2. Experimental Section

Materials. The surfactant AOT (99% purity) was purchased from Sigma. The isooctane, KBH_4, $AgNO_3$, and ethanol supplied by the Beijing Chemical Plant were all A. R. grade. Double-distilled water was used.

Synthesis of Ag Nanoparticles in Reverse Micelles. The procedures to synthesize Ag nanoparticles in the reverse micelles were similar to those reported by other authors.[62] A stock solution of 50 mmol/L AOT/isooctane was first prepared. The reverse micelle solutions containing aqueous solutions of $AgNO_3$ (0.5 mol/L) and KBH_4 (0.25mol/L) were prepared by adding the corresponding aqueous salt solution to the surfactant solution. The molar ratio of water to surfactant (w_0) is 10. The two micellar solutions containing $AgNO_3$ and KBH_4 were mixed, silver nanoparticles were formed in the reverse micelles, and the reverse micellar solution after mixing was treated immediately in the ultrasonic cleaning bath (240 Hz, 50 W) for the desired time. The temperature of the bath was controlled at 25 °C by a temperature controller (model HAAK D8). The reduction reaction of Ag^+ by BH_4^- in reverse micelles was described in detail in the literature.[62]

Silver Recovery and Characterization. The solvent isooctane was evaporated, and the deposits were washed repeatedly with ethanol and water to remove the surfactant and the byproducts. X-ray diffraction analysis of the samples was carried out using an X-ray diffractometer (XRD, model D/MAX2500, Rigaka) with Cu Kα radiation. The morphologies and the electron diffraction (ED) of the obtained particles were determined by transmission electron microscopy (TEM) with a HITACHI H-600A electron microscope. Particles were dispersed in ethanol and then directly deposited onto the copper grid.

UV Experiments. A UV sample cell was filled with the reverse micellar solution with Ag nanoparticles. Then, the sample cell was sealed and was placed in an ultrasonic cleaning bath (240 Hz, 50 W) filled with water at 25 °C. After the ultrasonication was carried out for a certain period of time, the UV spectrum of the reverse micellar solution was determined by a UV−vis spectrophotometer (model TU-1201).

SAXS Experiments. SAXS experiments were carried out at beamline 4B9A at the Beijing Synchrotron Radiation Facility (BSRF). The small-angle X-ray scattering station was located 31 m from the source. The station was equipped with a SAXS camera, a detector, an on-line data acquisition system, a controlling system, and an alignment carriage. The wavelength of the X-rays was 1.54 Å, and the sample-to-detector distance was 1.50 m. A detailed description of the spectrometer was given elsewhere.[63] In a typical experiment, the sample cell was filled with the micellar solution and treated by ultrasonication for a certain time, and then the X-ray scattering was recorded.

Data Analysis of SAXS. After correcting the scattering data by subtracting the background noise, the following analyses were done. In the lower-angle region, contributions to the total excess X-ray scattering, $I(\mathbf{h})$, due to microemulsions can arise from two sources: the droplet contribution, which depends solely upon the radius of the droplet, and an appropriate structure factor, which accounts for attractive or repulsive interactions between the droplets. When the system is sufficiently dilute, interdroplet interactions are negligible. The magnitude of the scattering vector $\mathbf{h}$ is given in terms of the scattering angle θ by $\mathbf{h} = 4\pi \sin \theta/\lambda$, where λ is the incident X-ray wavelength of 1.54 Å. For dilute solutions, the radius of gyration R_g of the micellar core can be obtained by using the Guinier approximation law, which is valid in the low-$\mathbf{h}$ region ($\mathbf{h}R_g < 1$) and can be expressed by eq 1:[56−58,64−68]

$$\ln[I(\mathbf{h})] = \ln[I(0)] - \frac{(\mathbf{h}R_g)^2}{3} \quad (1)$$

$I(0)$ denotes the scattering intensity extrapolated to zero angle. The Guinier plots give a precise value of the radius of gyration only if the representation is linear at small values of $\mathbf{h}$ where $\mathbf{h}R_g$ is less than 1. In this work, we use the method used by Hirai et al.[56,58] to obtain R_g (i.e., the R_g values are obtained by using a Guinier plot ($\ln I(\mathbf{h})$ vs $\mathbf{h}^2$) on the data sets in a defined small $\mathbf{h}$ range (0.02−0.03 Å^{-1})).

For monodispersed spherical particles, the theoretical SAXS scattering intensities can be represented by the following equations:[66−68]

$$I(\mathbf{h}) = I_e N n^2 \phi^2(\mathbf{h}R) \quad (2)$$

$$\phi^2(\mathbf{h}R) = \left[3\frac{\sin(\mathbf{h}R) - \mathbf{h}R\cos(\mathbf{h}R)}{(\mathbf{h}R)^3}\right]^2 \quad (3)$$

I_e denotes the scattering intensity per electron, N, the total number of particles irradiated by X-rays, and n, the number of electrons per particle. R is the true radius of the spherical particles and can be calculated from the radius of gyration by the following equation:

$$R_g = \sqrt{\frac{3}{5}}R \quad (4)$$

For ellipsoidal particles, the theoretical SAXS scattering intensities can be represented by the following equation:[66−68]

$$I(\mathbf{h}) = I_e N n^2 \left[\int_0^{\pi/2} \phi^2(\mathbf{h}a\sqrt{\cos^2\theta + \omega^2 \sin^2\theta})\cos\theta \, d\theta\right] \quad (5)$$

a and ω represents the minor semiaxes and the ratio of major to minor semiaxes, respectively. The value of a can be obtained from the relation with R_g:

$$R_g = a\left[\frac{2+\omega^2}{5}\right]^{1/2} \quad (6)$$

We used the procedure described by Z. F. Meng et al. to get information about the micellar shape.[67−68] The SAXS scattering curves are first simulated with different ω values according to the certain radius of gyration determined by the experiments. The intensities of the simulated and the experimental SAXS profiles were unified to a certain value. The detail of molecular arrangements in the aggregates is considered by comparing the scattering profiles calculated from the models with the observed SAXS profiles. The simulation process was conducted by using a Visual Basic program written by us.

3. Results and Discussion

Phase Structure and Morphologies of the Nanoparticles. The phase structure of the as-prepared nanoparticles is characterized by X-ray diffraction (XRD), as shown in Figure 1. XRD shows the presence of broad peaks corresponding to the nanocrystals, of which the four strong diffraction peaks correspond to the (110), (200), (220), and (311) planes. All of the peaks in the XRD can be indexed as a face-centered cubic (fcc)

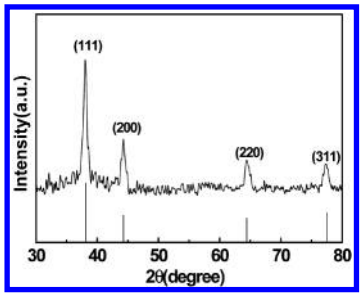

Figure 1. X-ray diffraction pattern of the obtained Ag after ultrasonication for 4 h. The vertical lines at the bottom indicate the standard position and relative intensities of fcc silver.

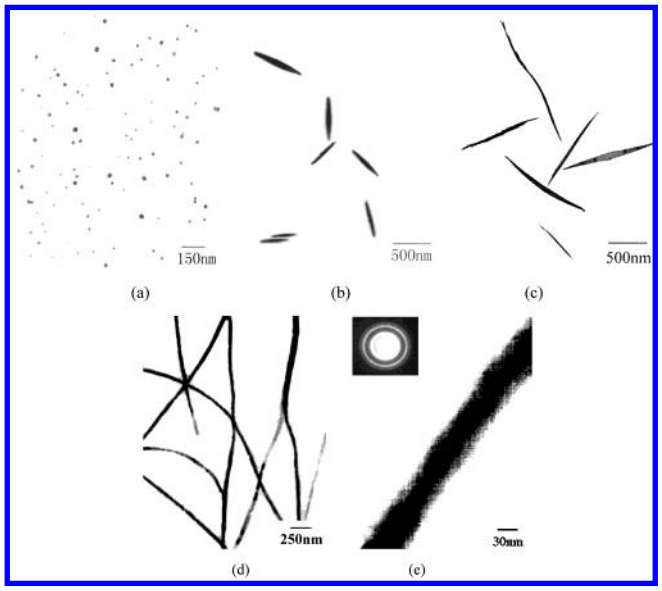

Figure 2. TEM photographs of Ag particles recovered from reverse micelles ([AOT] = 50 mmol/L, $w_0 = 10$) after different ultrasonication times (t): (a) 0, (b) 0.5 h, (c) 1 h, (d) 4 h, and (e) 4 h (with high magnification), with the inset plot representing its electron diffraction pattern.

structure (JCPDS no. 4-0783). No peaks of any other phase are detected, indicating the high purity of the product.

The TEM photographs of the silver particles recovered from the reverse micelles at different ultrasonication times are shown in Figure 2. The particle size can be obtained by measuring the diameter and the length of the particles in the micrographs. Figure 2a illustrates the TEM photographs of Ag nanoparticles recovered from the ultrasound-free reverse micelles ($w_0 = 10$, [AOT] = 50 mmol/L), which shows that only spherical nanoparticles of about 10−25 nm are obtained. However, by ultrasonic radiation, Ag particles of various morphologies are obtained; these are shown in Figure 2b−d. As we can see, at increasing ultrasonication time of 0.5 or 1 h, the needle-shaped particles can be obtained with length of <2 μm, and the length increases with ultrasonication time. Given enough time for ultrasonic radiation (t = 4 h), wire-shaped particles with diameters of about 50 nm and a length of 5 μm were obtained. In other words, the particle morphologies and sizes can be tuned via the ultrasonication time. Figure 2e gives a photograph of the wires shown in Figure 2d at a larger magnification, and the corresponding electron diffraction pattern for the wires is also indicated in Figure 2e. The characteristic rings in the diffraction pattern can be indexed to the (110), (200), (220), and (311) planes, allowed reflecting planes expected from the face-centered cubic (fcc) structure that are consistent with the diffraction peaks indexed in the XRD pattern.

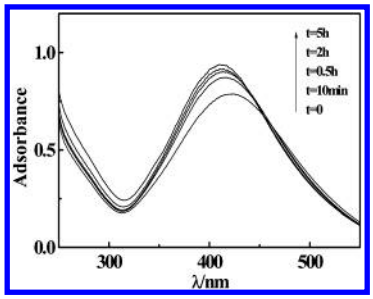

Figure 3. UV spectra of reverse micelles ([AOT] = 50 mmol/L, $w_0 = 10$, [Ag] = 1.2 mmol/L) containing Ag for various ultrasonication times (t).

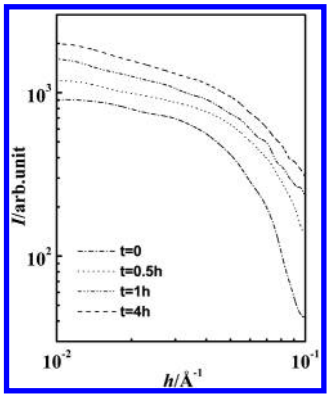

Figure 4. Experimental SAXS profiles of the reverse micelles ([AOT] = 50 mmol/L, $w_0 = 10$) at different ultrasonication times (t).

Effect of Ultrasoncation on Nanoparticles in Reverse Micelles by UV Spectra. The silver nanoparticles in reverse micelles can be characterized in situ by UV−vis spectra.[62,69−71] In Figure 3, some typical UV−vis spectra of Ag nanoparticles dispersed in reverse micelles ($w_0 = 10$, [AOT] = 50 mmol/L) are shown as a function of ultrasonication time. The very broad absorption band centered at about 420 nm is characteristic of nanosized Ag particles. In the absence of ultrasonication, the absorption spectrum is broad with a low optical density. However, after the solution is treated by ultrasonication, the absorption spectrum becomes narrower and slightly blue-shifted with an increase in the intensity of the plasmon band and a decrease in the bandwidth, especially in the first several minutes of ultrasonication. These changes in the Ag adsorption band may originate from the electromagnetic coupling of the particle assembles or aggregates into chains. In addition, it is well known that the maximum and the bandwidth of the absorption band depend on the surrounding medium of the particles. The microstructure of the reverse micelles should change with the aggregation of the nanoparticles because the silver nanoparticles are confined in the micellar cores. This may partially contribute to the change in the Ag adsorption band. These changes caused by ultrasonication are stable for a certain period of time, which is confirmed by the fact that the UV spectra is unchanged after the cessation of ultrasonication for several days.

Effect of Ultrasonication on the Microstructure of Micelles. To obtain some information about the mechanism of ultrasonication, we determined the SAXS curves of the nanoparticle-free reverse micelles (water/AOT/isooctane) before and after ultrasonication. As examples, Figure 4 shows some typical SAXS curves of reverse micellar solutions ([AOT] = 50 mmol/L, $w_0 = 10$) before and after ultrasonication for a certain period of time. In the small-angle region, the scattering intensity is increased by ultrasonication treatment. One of the reasons is that micellar size increases by ultrasonication, which is confirmed by the radius of gyration R_g discussed in the following

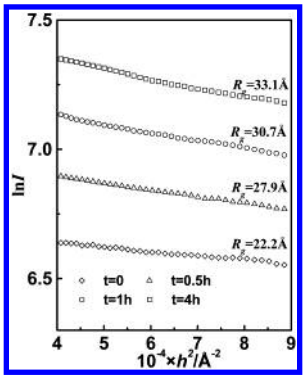

Figure 5. Dependence of Guinier plots of reverse micelles ([AOT] = 50 mmol/L, $w_0 = 10$) on ulrasonication time (t).

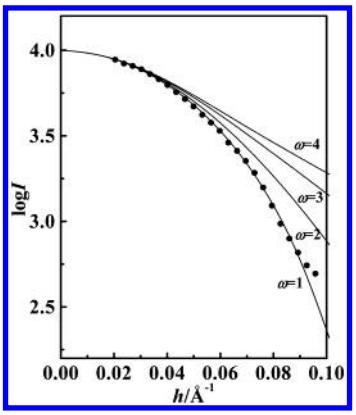

Figure 6. Typical simulated SAXS profiles with various ω (—) and experimental SAXS profiles (●) for reverse micelles in the absence of ultrasonication.

section. The Guinier plots of $\mathbf{h}^2 \sim \ln I(\mathbf{h})$ show good linearity in the $\mathbf{h}^2$ range of 0.0004−0.0009 Å^{-2}, which is shown in Figure 5. It is evident that ultrasound can cause an increase in the radius of gyration of the micelles.

Using eqs 2−6, we have simulated the SAXS curves with various ω values for the above systems corresponding to a certain radius of gyration. The theoretical scattering functions of ellipsoidal particles are fit to the experimental scattering functions. As examples, Figure 6 shows experimental SAXS profiles for reverse micelles in the absence of ultrasonication and the typical simulated SAXS profiles with various ω values. As we can see, with the increase in ω, the slope of the simulated scattering curves progressively decreases, distinguishing the spheres from the ellipsoids. It is clear that the experimental curve agrees with the simulated curve of $\omega = 1$ in the small-angle region, which indicates spherical droplets with radius of $R =$ 28.7 Å in the absence of ultrasonication.

Figure 7 shows experimental SAXS profiles and the typical simulated SAXS profiles for reverse micelles after ultrasonication for various times. As can be seen, for the reverse micelles after ultrasonication for 0.5, 1, and 4 h, the experimental scattering curves show good consistency with the calculated curves of $\omega = 1.9$, 2.3, and 2.6, respectively. The corresponding lengths of the minor and major semiaxes for these three systems are 26.3 and 50.0 Å, 25.4 and 58.4 Å, and 25.0 and 65.0 Å, respectively. This indicates that the ultrasonication results in the micellar transition from a spherical to an ellipsoidal structure and that the micelles become more ellipsoidal with increasing ultrasonication time, which is characterized by the increase in ω. The reason may be that the microjet and shock-wave impacts of ultrasound activate the surfactant/water interface and improve the mass transfer through the boundary layer. We believe that

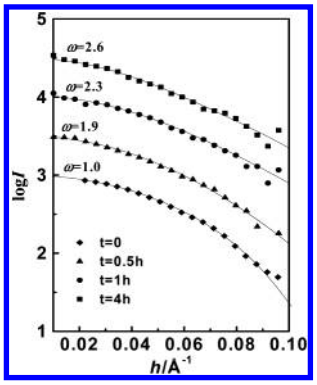

Figure 7. Typical simulated SAXS profiles (—) and experimental SAXS profiles (symbols) for reverse micelles([AOT] = 50 mmol/L, $w_0 = 10$) after ultrasonication for various times.

the microstructure change in the reverse micelles caused by ultrasonication is one of the main factors that induces the formation of the needle-shaped or wire-shaped particles.

The size of the prepared silver particles increases much more significant than that of the reverse micelles with the increase in ultrasonication time. This is reasonable because there were no Ag particles in the reverse micelles in the SAXS experiments. In the presence of the Ag particles, the reassembly of the surfactants caused by ultrasonication induces the aggregation of the Ag particles in the reverse micelles, which in turn affects the reassembly of the surfactants. In other words, the reassembly of the surfactants and the aggregation of Ag particles confined in the micellar cores promote each other, and thus the size change of the nanofiber is much more significant than that of the reverse micelles in the absence of the metal particles. Therefore, the SAXS results can provide information only about the microstructure change in the reverse micelles induced by ultrasonication, which can partially explain the formation of the nanorods and nanofibers. However, quantitative comparisons of the size of the reverse micelles and that of the prepared nanoparticles are meaningless.

Conclusions

In this work, we have successfully synthesized silver nanorods and nanofibers from AOT/isooctane reverse micelles with the aid of low-intensity ultrasonication. Direct microstructural information about the reverse micelles after ultrasonication is provided by small-angle X-ray scattering. The introduction of ultrasonication into the solution results in the reassembly of AOT molecules and the micelle transition from a spherical to an ellipsoidal structure. In other words, the shape and size of the reverse micelles can be tuned via the ultrasonication time, which is coupled to the aggregation of nanoparticles dispersed in the reverse micelles. Such an ultrasonication-based approach provides a new route to the synthesis of nanorods and nanofibers directly from the reverse micelles, which largely simplifies the experimental process compared to other methods.

Acknowledgment. This work was supported by the Ministry of Science and Technology (G2000078103) and the National Natural Science Foundation of China (20133030).

References and Notes

(1) Moreno-Manas, M.; Pleixats, R.; Villarroya, S. *Chem. Commun.* **2002**, 60.

(2) Lemon, B. I.; Crooks, R. M. *J. Am. Chem. Soc.* **2000**, *122*, 12886.

(3) Li, Y. M.; Kim, W.; Zhang, Y. G.; Rolandi, M.; Wang, D. W.; Dai, H. J. *J. Phys. Chem. B* **2001**, *105*, 11424.

(4) Loscertales, I. G.; Barrero, A.; Guerrero, I.; Cortijo, R.; Marquez, M.; Ganan-Calvo, A. M. *Science (Washington, D.C.)* **2002**, *295*, 1695.
(5) Ohde, H.; Wai, C. M.; Kim, H.; Kim, J.; Ohde, M. *J. Am. Chem. Soc.* **2002**, *124*, 4540.
(6) Yeung, L. K.; Lee, C. T.; Johnston, K. P.; Crooks, R. M. *Chem. Commun.* **2001**, 2290.
(7) Sau, T. K.; Pal, A.; Pal, T. *J Phys. Chem. B* **2001**, *105*, 9266.
(8) Wuelfing, W. P.; Green, S. J.; Pietron, J. J.; Cliffel, D. E.; Murray, R. W. *J. Am. Chem. Soc.* **2000**, *122*, 11465.
(9) Trindade, T.; O'Brien, P.; Pickett, N. L. *Chem. Mater.* **2001**, *13*, 3843.
(10) Poizot, P.; Laruelle, S.; Grugeon, S.; Dupont, L.; Tarascon, J. M. *Nature (London)* **2000**, *407*, 496.
(11) Kurth, N.; Renard, E.; Brachet, F.; Robic, D.; Guerin, P.; Bourbouze, R. *Polymer* **2002**, *43*, 1095.
(12) Niemeyer, C. M. *Angew. Chem., Int. Ed.* **2001**, *40*, 4128.
(13) Caruso, F.; Schuler, C. *Langmuir* **2000**, *16*, 9595.
(14) Muster, J.; Kim, G. T.; Krstic, V.; Park, J. G.; Park, Y. W.; Roth, S.; Burghard, M. *Adv. Mater.* **2000**, *12*, 420.
(15) Duan, X. F.; Lieber, C. M. *J. Am. Chem. Soc.* **2000**, *122*, 188.
(16) Pan, Z. W.; Dai, Z. R.; Wang, Z. L. *Science (Washington, D.C.)* **2001**, *291*, 1947.
(17) Huang, Y.; Duan, X. F.; Cui, Y.; Lauhon, L. J.; Kim, K. H.; Lieber, C. M. *Science (Washington, D.C.)* **2001**, *294*, 1313.
(18) Matsui, K.; Pradhan, B. K.; Kyotani, T.; Tomita, A. *J. Phys. Chem. B* **2001**, *105*, 5682.
(19) Fullam, S.; Cottell, D.; Rensmo, H.; Fitzmaurice, D. *Adv. Mater.* **2000**, *12*, 1430.
(20) Govindaraj, A.; Satishkumar, B. C.; Nath M., Rao, C. N. R. *Chem. Mater.* **2000**, *12*, 202.
(21) Cao, H. Q.; Xu, Y.; Hong, J. M.; Liu, H. B.; Yin, G.; Li, B. L.; Tie, C. Y.; Xu, Z. *Adv. Mater.* **2001**, *13*, 1393.
(22) Cao, H. Q.; Xu, Z.; Wei, X. W.; Ma, X.; Xue, Z. L. *Chem. Commun.* **2001**, 541.
(23) Nielsch, K.; Muller, F.; Li, A. P.; Gosele, U. *Adv. Mater.* **2000**, *12*, 582.
(24) Nguyen, P. P.; Pearson, D. H.; Tonucci, R. J.; Babcock, K. *J. Electrochem. Soc.* **1998**, *145*, 247.
(25) Berry, A. D.; Tonucci, R. J.; Fatemi, M. *Appl. Phys. Lett.* **1996**, *69*, 2846.
(26) Suslick, K. S.; Price, G. J. *Annu. Rev. Mater. Sci.* **1999**, *29*, 295.
(27) Cintas, P.; Luche, J. L. *Green Chem.* **1999**, *1*, 115.
(28) Nunes, O. A. C.; Fanyao, Q.; Santos, W.; Fonseca, A. L.; Agrello, D. *J. Appl. Phys.* **1998**, *84*, 2420.
(29) Shafi, K. V. P. M.; Ulman, A.; Dyal, A.; Yan, X. Z.; Yang, N. L.; Estournes, C.; Fournes, L.; Wattiaux, A.; White, H.; Rafailovich, M. *Chem. Mater.* **2002**, *14*, 1778.
(30) Langer, R. *Acc. Chem. Res.* **2000**, *33*, 94.
(31) Johnson, L. L.; Peterson, R. V.; Pitt, W. G. *J. Biomater. Sci., Polym. Ed.* **1998**, *9*, 1177.
(32) Hiorns, R. C.; Khoukh, A.; Ghigo, P.; Prim, S.; Francois, J. *Polymer* **2002**, *43*, 3365.
(33) Kim, H.; Lee, J. W. *Polymer* **2002**, *43*, 2585.
(34) Liao, Y. Q.; Wang, Q.; Xia, H. S.; Xu, X.; Baxter, S. M.; Slone, R. V.; Wu, S. G.; Swift, G.; Westmoreland, D. G. *J. Polym. Sci., Polym. Chem. Ed.* **2001**, *39*, 3356.
(35) Wang, H.; Zhu, J. J.; Zhu J. M.; Chen, H. Y. *J. Phys. Chem. B* **2002**, *106*, 3848.
(36) Kumar, R. V.; Koltypin, Y.; Xu, X. N.; Yeshurun, Y.; Gedanken A.; Felner, I. *J. Appl. Phys.* **2001**, *89*, 6324.
(37) Koltypin, Y.; Nikitenko, S. I.; Gedanken, A. *J. Mater. Chem.* **2002**, *12*, 1107.
(38) Nikitenko, S. I.; Koltypin, Y.; Mastai, Y.; Koltypin, M.; Gedanken, A. *J. Mater. Chem.* **2002**, *12*, 1450.
(39) Cooper, A. I. *Adv. Mater.* **2001**, *13*, 1111.
(40) Simmons, B. A.; Li, S. C.; John, V. T.; McPherson, G. L.; Bose, A.; Zhou, W. L.; He, J. B. *Nano Lett.* **2002**, *2*, 263.
(41) Meziani, A.; Touraud, D.; Zradba, A.; Pulvin, S.; Pezron, I.; Clausse, M.; Kunz, W. *J. Phys. Chem. B* **1997**, *101*, 3620.
(42) Khomutov, G. B. *Colloids Surf., A* **2002**, *202*, 243.
(43) Li, M.; Mann, S. *Langmuir* **2000**, *16*, 7088.
(44) Lee, J. K.; Koh, W. K.; Chae, W. S.; Kim, Y. R. *Chem. Commun.* **2002**, 138.
(45) Rees, G. D.; Evans-Gowing, R.; Hammond, S. J.; Robinson, B. H. *Langmuir* **1999**, *15*, 1.
(46) Qi, L. M.; Ma, J. M.; Cheng, H. M.; Zhao, Z. G. *J. Phys. Chem. B* **1997**, *101*, 3460.
(47) Liu, J.; Teo, W. K.; Chew, C. H.; Gan, L. M. *J. Appl. Polym. Sci.* **2000**, *77*, 2785.
(48) Chew, C. H.; Li, T. D.; Gan, L. H.; Quek, C. H.; Gan, L. M. *Langmuir* **1998**, *14*, 6068.
(49) Aikawa, K.; Kaneko, K.; Tamura, T.; Fujitsu, M.; Ohbu, K. *Colloids Surf., A* **1999**, *150*, 95.
(50) Zhao, H. Y.; Douglas, E. P. *Chem. Mater.* **2002**, *14*, 1418.
(51) Liu, T. B.; Xie, Y.; Chu, B. *Langmuir* **2000**, *16*, 9015.
(52) Cepak, V. M.; Martin, C. R. *J. Phys. Chem. B* **1998**, *102*, 9985.
(53) Chen, C. W.; Chen, M. Q.; Serizawa, T.; Akashi, M. *Adv. Mater.* **1998**, *10*, 1122.
(54) Wang, C. Y.; Chen, M. H.; Zhu, G. M.; Lin, Z. G. *J. Colloid Interface Sci.* **2001**, *243*, 362.
(55) Wu, S. D.; Zhu, Z. G.; Tan, J. Y.; Gao, J. C. *Chem. Lett.* **2001**, *5*, 396.
(56) Hirai, M.; Kawai-Hirai, R.; Yabuki, S.; Takizawa, T.; Hirai, T.; Kobayashi, K.; Amemiya Y.; Oya, M. *J. Phys. Chem.* **1995**, *99*, 6652.
(57) Liu, J. C.; Han, B. X.; Zhang, J. L.; Li, G. Z.; Zhang, X. G.; Wang, J.; Dong, B. Z. *Chem. Eur. J.* **2002**, *8*, 1356.
(58) Hirai, M.; Kawai-Hirai, R.; Sanada, M.; Iwase H.; Mitsuya, S. *J. Phys. Chem. B* **1999**, *103*, 9658.
(59) Rancesca, C.; Giulia, C.; Piero, B.; Maura, M. *J. Phys. Chem. B* **1997**, *101*, 10205.
(60) Bardez, E.; Nguyen, C. V. *Langmuir* **1995**, *11*, 3374.
(61) Fulton, J. L.; Pfund, D. M.; Desimone, J. M.; Capel, M. *Langmuir* **1995**, *11*, 4241.
(62) Barnickel, P.; Wokaun, A.; Sager, W.; Eicke, H. F. *J. Colloid Interface Sci.* **1992**, *148*, 80.
(63) Dong, B. Z.; Sheng, W. J.; Yang, H. L.; Zhang, Z. J. *J. Appl. Crystallogr.* **1997**, *30*, 877.
(64) Eastoe, J.; Paul, A.; Nave, S.; Steytler, D. C.; Robinson, B. H.; Rumsey, E.; Thorpe, M.; Heenan, R. K. *J. Am. Chem. Soc.* **2001**, *123*, 988.
(65) Maitra, A. *J. Phys. Chem.* **1984**, *88*, 5122.
(66) Guinier, A. *X-ray Diffraction*; University of Paris: Paris, France, 1963; p 323.
(67) Meng, Z. F. *Theory and Application of Small-Angle X-ray Scattering*; Jilin Science and Technology Press: Jilin, China, 1996; p 311.
(68) Meyer, W. R.; Pulcinelli, S. H.; Santilli, C. V.; Craievich, A. F. *J. Non-Cryst. Solids* **2000**, *273*, 41.
(69) Petit, C.; Lixon, P.; Pileni, M. P. *J. Phys. Chem.* **1993**, *97*, 12974.
(70) Charlé, K. P.; Schulze, W. *Ber. Bunsen-Ges. Phys. Chem.* **1984**, *88*, 350.
(71) Kawabata, A.; Kubo, R. *J. Phys. Soc. Jpn.* **1966**, *21*, 1765.